Journal of RAMAN SPECTROSCOPY

High-pressure Raman spectroscopy of $Ca(Mg,Co)Si_2O_6$ and $Ca(Mg,Co)Ge_2O_6$ clinopyroxenes

Journal:	*Journal of Raman Spectroscopy*
Manuscript ID	JRS-16-0320.R2
Wiley - Manuscript type:	Research Article
Date Submitted by the Author:	n/a
Keywords:	micro-Raman spectroscopy, high pressure, pyroxenes, germanates, silicates

Complete List of Authors:
Bersani, Danilo; University of Parma, Physics and Earth Sciences
Tribaudino, Mario; Scienze della Terra
Aliatis, Irene; Universita degli Studi di Parma, Physics and Earth Sciences
Gatta, Giacomo; Universita degli Studi di Milano, Scienze della terra
Lambruschi, Erica; Universita degli Studi di Parma, Physics and Earth Sciences
Mantovani, Luciana; University of Parma, Department of Physics and Earth Sciences
Redhammer, Guenther; University of Salzburg, Department of Materials Science & Physics, Division of Mineralogy
Lottici, Pier Paolo; University, Physics and Earth Sciences

High-pressure Raman spectroscopy of $Ca(Mg,Co)Si_2O_6$ and $Ca(Mg,Co)Ge_2O_6$ clinopyroxenes

[1]M. Tribaudino, [1]I. Aliatis, [1]D. Bersani*, [2]G. D. Gatta, [1]E. Lambruschi, [1]L. Mantovani, [3]G. Redhammer, [1]P. P. Lottici

[1] Università di Parma, Dipartimento di Fisica e Scienze della Terra, Parco Area delle Scienze 7/A, 43124 Parma, Italy

[2] Università degli Studi di Milano, Dipartimento di Scienze della Terra, Via Botticelli 23, 20133 Milano, Italy

[3] Universitaet Salzburg, Materialforschung und Physik, Hellbrunnerstrasse 34, 5020 Salzburg, Austria

danilo.bersani@fis.unipr.it

Abstract

In situ high-pressure Raman spectra were collected on four pyroxenes, with composition $CaCoSi_2O_6$, $CaMgSi_2O_6$, $CaCoGe_2O_6$ and $CaMgGe_2O_6$ and, up to P = 7.6 and 8.3 GPa, for silicates and germanates, respectively. The peak wavenumbers υ_i increase almost linearly with pressure; the slope $d\upsilon_i/dP$ is more pronounced for the modes at higher wavenumbers, and higher in germanates than in silicates. No phase transition or change in the compressional behaviour was observed within the P-range investigated. The strong dependence of the peak position with pressure of the high energy stretching modes is due to the high sensitivity of the vibrational frequencies probed by Raman spectroscopy to subtle changes in the tetrahedral deformation, which are overlooked by single crystal X-ray diffraction.

Keywords: micro-Raman spectroscopy, high pressure, pyroxenes, germanates, silicates.

Introduction

Pyroxenes, being major phases in Earth mantle, have been the object of several in situ high-pressure investigations: vibrational and elastic properties were measured often on the basis of crystal structure refinements [1-13]. The phase transitions discovered in the high-pressure experiments gave hints to the geophysical modelling of the velocity of the seismic waves at the

mantle boundaries, and proved to be crucial to interpret the evolution of the structural deformations in silicates [2, 14-21].

Raman spectroscopy is one of the most suitable techniques for the investigation of the vibrational behaviour of minerals at high pressure. Phase transitions are readily revealed, in some cases even before the same transitions are confirmed by in situ high-pressure X-ray diffraction [7, 22-24]. Another advantage is that Raman peaks are related to specific structural features, providing clues on structural deformations alternative to the more time-consuming in situ single-crystal X-ray diffraction investigations [25, 26]. The potential of Raman spectroscopy in unravelling subtle structural features was recently improved by detailed quantum mechanical analysis in pyroxenes: the careful description of the vibrational dynamics, now available for pyroxenes, may relate specific vibrational modes to the structural changes [26, 27].

The rather flexible structure of pyroxenes allows large deformation with pressure and temperature. For instance, in the holotypic diopside ($CaMgSi_2O_6$), the pyroxene structure can be deformed without any transformation at pressure beyond 50 GPa, and only at 53 GPa it transforms into an ilmenite-like structure [29]. Moreover, in natural and synthetic pyroxenes widespread solid solutions are possible.

The structural unit formula of pyroxenes is $M2M1T_2O_6$: the M2 site, hosted in a distorted 6-8 fold coordinated polyhedron, can be populated by Ca, Na, Mg, Fe, Li, Co, Mn, Zn; the M1 site, in an almost regular octahedron, by Mg, Mn, Fe, Cr, Ti, Zn, Co, Ni, Sc, In, Ga, Al; the T tetrahedral site by Si, Ge, and, in part, by Al.

Most studies concerned Si pyroxenes. Ge pyroxenes, and more in general Ge-silicates were the object of extensive investigation only in the pioneering studies on phase transitions in the Earth mantle [30, 31]. At the time, the high-pressure conditions expected in the mantle could not be achieved experimentally, and germanates were used as model systems instead of the isomorphic silicates, as phase transitions occur at lower pressure in germanates than in silicates.

Recently, there has been a reappraisal for studies aiming to the systematic analysis of the evolution of structural parameters and physical properties in pyroxenes. Being Ge the only cation that can fully replace Si in pyroxenes, any investigation on Ge-pyroxenes will give important hints to model the behaviour of the T tetrahedron in pyroxenes. In addition, as a by-product, several innovative phase transitions were observed in Ge pyroxenes [32-34]. In situ high-pressure studies are however scarce and most limited to X-ray diffraction structure refinements and elastic behaviour of Ge-pyroxenes. To our knowledge, the only study reporting Raman spectra of Ge-pyroxenes at high pressure was performed by Hofer et al. [35] for $LiScGe_2O_6$ and $NaScGe_2O_6$ and no attempt was made to compare the results on Ge-pyroxenes with the Si-counterparts.

In this work, we report the high-pressure Raman measurements on two end member Ge-pyroxenes, $CaMgGe_2O_6$ and $CaCoGe_2O_6$, and of their Si-counterparts, $CaMgSi_2O_6$ and $CaCoSi_2O_6$, comparing the pressure dependence of the Raman modes in Mg and Co germanate and silicate pyroxenes.

Experimental methods

An ETH-type diamond anvil cell (DAC) [36] was used for the high-pressure Raman experiments. Stainless-steel T301 foil, 250 μm thick, pre-indented to a thickness of about 100 μm, with a 300 μm hole obtained by electro-spark erosion, was used as a gasket. Type-II diamonds were used as anvils (culet ∅ 600 μm). Natural diopside [37], with composition $CaMg_{0.93}Fe_{0.07}Si_2O_6$, synthetic $CaCoSi_2O_6$ [38, 39], and $CaCoGe_2O_6$ [40] single crystals were loaded in the DAC for the experiments. $CaMgGe_2O_6$ was available only as a polycrystalline material [40], and a few crystallites (average size 8-10 μm) were loaded in the *P*-chamber. Therefore, the absolute intensities of the Raman modes in $CaMgGe_2O_6$ could be affected by the orientation of the crystallites.

Silicate and germanate pyroxenes were loaded in two separate runs, so that $CaCoSi_2O_6$ and $CaMgSi_2O_6$, and $CaMgGe_2O_6$ and $CaCoGe_2O_6$ experienced the same pressure, respectively. The crystals were placed in the gasket hole together with some ruby chips for pressure measurements by the ruby-fluorescence method (precision of ± 0.05 GPa according to Mao et al. [41]). Methanol: ethanol = 4:1 mixture was used as hydrostatic pressure-transmitting medium [42]. Raman spectra were collected in the pressure range 0.0001-7.6 GPa for silicates and 0.0001-8.27 for germanates, using an Olympus BX40 microscope attached to a Jobin-Yvon Horiba LabRam confocal Raman spectrometer, equipped with a charge-coupled detector (CCD). The samples were excited with the 473.1 nm blue light of a diode pumped Nd:YAG laser. The laser beam was focused on the sample on a spot of about 1.5 μm diameter (50x ultra long working distance objective, NA = 0.55) and the confocal aperture was set at 150 μm. The spectra were collected in backscattered geometry, in the spectral range 100-1000 cm^{-1}, with 600 s counting time and three accumulations. The spectrometer was calibrated using the emission lines of a spectroscopic Zn lamp. No special care was taken to enhance or minimize possible polarization effects. Raman peak profiles were integrated using pseudo-Voigt functions.

Results and discussion

The crystal structures of the studied pyroxenes are described in the *C*2/*c* space group and are quite similar, with small differences in the bond distances and polyhedral distortion [40]. Pyroxenes are made of tetrahedral chains, generated four times by symmetry in the unit cell, connected by a ribbon of edge sharing M1 octahedra and by the M2 cations in a distorted 8-fold configuration (Fig. 1). Factor-group analysis at Γ point (**k**=0) shows that *C*2/*c* pyroxenes, with 20 atoms in the reduced primitive unit cell ($Z = 2$), have 30 (14 A_g + 16 B_g) Raman active modes [43, 26].

Recent quantum mechanical calculation of the vibrational modes in diopside and orthoenstatite [27, 28] showed that the vibrational modes are a complex mixture of bending and stretching-like vibrations involving different atoms: in general, almost pure stretching modes may be found only at wavenumbers higher than 1000 cm^{-1}. In terms of prevailing mode vibration, in the wavenumber range below 500 cm^{-1}, modes associated with cation translations as well as longer-wavelength lattice modes are found; the different response of the vibrational modes to changes in pressure, temperature and composition depends on whether they are involved in structural changes of the M1 or M2 polyhedra. The peaks in the mid wavenumber region, between 500 and 800 cm^{-1}, are associated to inter-tetrahedral stretching and bending modes of the tetrahedral chain, with a significant influence of M1 and M2 cation bonding. The modes at higher wavenumbers are associated to Si–O stretching modes of the non-bridging oxygens, i.e. those not shared between tetrahedra along the chain.

The spectra of the investigated silicates show few major peaks between 300 and 400 cm^{-1}, mostly related to stretching and bending in the M2 and M1 polyhedra, a single feature at ~ 670 cm^{-1} and another intense peak at about 1010 cm^{-1}, related to bending and stretching of the tetrahedra, respectively. In germanates, we find similar features albeit downshifted in energy [41]. The strong peaks at ~670 and ~1010 cm^{-1} in silicates have their counterpart at ~550 cm^{-1} and ~850 cm^{-1} in germanates, respectively [40]. In germanates, the peak corresponding to that at about 1010 cm^{-1} in silicates is accompanied by a second peak at lower intensity.

The weak Raman features that can hardly be followed throughout the high-pressure runs were not considered in this study, thus reducing the number of described peaks with respect to those reported by Chopelas and Serghiou [7]. Only the peak positions of six strong peaks could be followed both in $CaCoSi_2O_6$ and in $CaMgSi_2O_6$. In $CaMgGe_2O_6$ and $CaCoGe_2O_6$, 16 and 11 peaks could be clearly identified. Among them, the peak positions of 13 and 9 peaks, respectively, were followed with pressure.

The relative intensity of the peaks varies considerably with pressure, but, as the measurement spot may change during measurements, it is not possible to discriminate the effect of pressure or orientation on the relative intensities.

We found that the wavenumbers ν_i of the Raman features increase linearly with increasing pressure: the derived slopes $d\nu_i/dP$ are reported in Table 1. The deviation from linear behaviour observed in diopside, in response to the non-linear volume and structural changes with pressure [7] was not detected in our experiments, for the limited *P*-range of investigation.

With increasing pressure, the peak positions vary smoothly and no sudden change in the slope $d\nu_i/dP$ (which may be indicative of a change in the compressional behaviour), nor appearance of extra peaks (which may be indicative of a phase transition) was observed (Fig. 1-2). A change of the compressional behaviour was found in diopside at pressure higher than those of this study, both by Raman spectroscopy and X-ray diffraction [5,7]; moreover, at $P > 53$ GPa a reversible transition to the ilmenite structure occurs [44].

The smooth increase in wavenumber with pressure found for all peaks corresponds to the decreased unit-cell volume. The low energy modes between 150 and 200 cm^{-1} in germanates show small variations. Intermediate modes show $d\nu_i/dP$ between 2.5 and 3.5 cm^{-1}/GPa. The tetrahedral stretching modes show higher *P*-induced variations, between 3.9 and 5.3 cm^{-1}/GPa. In diopside, the volumes of the M1 and M2 polyhedra decrease by 7.8 and 8.0%, respectively, in the range 0.0001 to 10.16 GPa, whereas that of Si tetrahedron decreases by only 2.7% [12]. Even if small, the decrease in Si-O bonds distances with pressure has a significant effect.

The high effect on the Raman peak positions of small changes in interatomic distances in tetrahedra, hardly detected in the structure refinements based on high-pressure single-crystal X-ray diffraction data, was observed also in the orthopyroxene enstatite [28].

The same is found for pyroxenes of the series $CaMgSi_2O_6$ - $CaCoSi_2O_6$, where the structural changes in the tetrahedron are negligible by single-crystal X-ray diffraction [45], and the tetrahedral bond lengths appear to be unchanged in all the series. The strong changes in higher wavenumber modes have been related only to small differences in the tetrahedral distortion [46].

In the description of the high pressure behaviour of the studied pyroxenes, we will compare separately the differences between Co and Mg pyroxenes with the same cation at the tetrahedral site, and those between Ge and Si pyroxenes with the same cation at the M1 site.

Between Co and Mg pyroxenes, the difference in $d\nu_i/dP$ of the corresponding Raman peaks is modest. Usually, Mg end-members show a slightly higher $d\nu_i/dP$ for peaks at lower wavenumber (Tab. 1-2). For the Si-O stretching modes, which were ascribed mainly to the stretching of Si-O with non-bridging oxygen sites [27], the difference between Co and Mg pyroxenes is not

significant, whereas in germanates the two Ge-O stretching peaks display evident differences between Co- and Mg-members. The main peak in germanates shows a $d\nu_i/dP$ in the Mg end-member, higher than in the Co end-member (5.3 cm^{-1}/GPa compared to 4.9 cm^{-1}/GPa). The opposite is true for the secondary peak, with the 809 cm^{-1} peak of Co pyroxene showing a $d\nu_i/dP$ higher than that observed for the 828 cm^{-1} peak of the Mg pyroxene (*i.e.*, 5.0 cm^{-1}/GPa *vs.* 3.9 cm^{-1}/GPa, respectively).

Comparing Ge- and Si-pyroxenes, we observe that the *P*-induced variation of the most intense and resolved stretching modes is significantly higher in germanates than in silicates (Table 1-2, Fig. 3), whereas for lower wavenumber peaks we did not find significant differences.

The higher *P*-induced variations of Mg- *vs.* Co-pyroxenes in intermediate wavenumber modes and of Ge- *vs.* Si-pyroxenes in higher wavenumber modes are likely related to the different compressional behaviour of the polyhedron hosting Co or Mg and of the tetrahedron hosting Ge or Si: we can expect that higher polyhedral compression is correlated to higher variation of Raman modes (ascribable to the polyhedral vibrations). Any interpretation would, therefore, need in situ high-pressure structural data, which, among the investigated phases, are available only for diopside [1,12]. Therefore, some assumptions will be done here, from the behaviour of pyroxenes with compositions similar to those of this study.

About the higher $d\nu_i/dP$ of intermediate wavenumber modes of Mg- *vs.* Co-pyroxenes, a first observation is that the unit-cell volume of the $CaMgSi_2O_6$ pyroxene is more compressible than in pyroxenes where Mg is replaced by a transition metal as Fe, Ni, Mn or Zn [35]. This was observed by comparing the unit-cell volume *vs*. the volume compression at 10 GPa in a series of pyroxenes; transition metal pyroxenes plot in a common trend, all with lower compressibility than $CaMgSi_2O_6$ pyroxene [35]. In addition, the M1 polyhedron is more compressible when it is populated by Mg rather than by Fe: the M1 volume compressibility is $7.7(2) \cdot 10^{-3}$ and $6.8(3) \cdot 10^{-3}$ GPa^{-1} in $CaMgSi_2O_6$ and $CaFeSi_2O_6$, respectively [12,47]. From our observations on Raman modes, we may assume that Co behaves as Fe and other transition metals, and that the M1 polyhedron is less compressible when occupied by Co than when it is populated by Mg.

Structural observations could also explain the very similar *P*-induced variation of the higher wavenumber stretching modes in $CaCoSi_2O_6$ and $CaMgSi_2O_6$, which could be ascribed to a very similar tetrahedral compression for the two phases. Again, we may compare $CaFeSi_2O_6$ and $CaMgSi_2O_6$: between 0.0001 and 10 GPa, the tetrahedral volume decreases by the same amount of 0.063 $Å^3$. This is predictable, as the tetrahedral site is fully populated by Si, and we may assume that also in $CaCoSi_2O_6$ the Si-tetrahedron experiences the same tetrahedral compression. On the

other side, it is not clear the origin of the difference observed in the higher wavenumber Ge-O stretching modes (Fig. 3).

The differences between silicates and germanates at higher wavenumber likely involve differences in the tetrahedral compression. In GeO_2, structurally analogous to α-quartz, the structure is compressed mainly by a deformation of the tetrahedral framework, with very little intra-tetrahedral compression. Yet, in the comparative paper by Glinnemann et al. [48], the reported average tetrahedral bond distances show a higher compression in germanates than in silicates, $4.1(1.2)\cdot10^{-4}$ *vs.* $2.1(4)\cdot10^{-4}$ GPa^{-1}. In pyroxenes, we do not have a similar example, *i.e.* a couple of pyroxenes different only for the Si *vs.* Ge substitution. A close example for comparison is that of *C*2/*c* $NaAlSi_2O_6$ and $NaScGe_2O_6$, where good quality data are available [35, 49]. Assuming that, as we found, the effect of the M1 polyhedron is negligible on the higher wavenumber modes, we may compare the different compressibility of the average T-O bond lengths. The values of compressibility in $NaAlSi_2O_6$ and $NaScGe_2O_6$, are $8.8(7)\cdot10^{-4}$ and $11.2(5)\cdot10^{-4}$ GPa^{-1}, respectively, which support the indication of a higher tetrahedral compression in Ge-pyroxenes.

Conclusions

The high-pressure Raman spectra of the pyroxenes $CaMgGe_2O_6$ and $CaCoGe_2O_6$, and $CaMgSi_2O_6$ and $CaCoSi_2O_6$ did not show evidence either of a phase transition or a change in compressional behaviour at least up to 8 GPa. The structures apparently keep the *C*2/*c* space group within the investigated *P*-range. A phase transition in the Ca-germanate members could be expected, as diopside experiences a phase transition at pressure in excess of 10 GPa [44], and a lower transition pressure is expected in isotypic germanates; such a transition was not observed in this study.

A slightly higher compression of Mg- with respect to Co-pyroxenes was observed in lower energy modes (irrespective of the tetrahedral population), likely related to a different compression of the M1 polyhedron. Such a difference almost disappears for higher energy modes, which are most or completely related to tetrahedral bond stretching.

A higher compression of the tetrahedral Ge-O bonds than the Si-O counterparts is here inferred, on the basis of the significantly higher *P*-induced variation of the corresponding modes at higher wavenumbers. The tetrahedral compression is hardly observed by in situ X-ray single crystal diffraction, especially in the *P*-range 0.0001-10 GPa, whereas Raman spectroscopy appears as a suitable technique to model slight changes in intra-tetrahedral configurations.

References

[1] L. Levien, C.T. Prewitt, *Am. Mineral*. **1981** ; 66, 315.

[2] R.J. Angel, A. Chopelas, N.L. Ross, *Nature* **1992** ; 358, 322.

[3] R.J. Angel, D.A. Hugh-Jones, *J. Geophys. Res*. **1994** ; 99, 19777.

[4] H. Yang, L.W. Finger, P.G. Conrad, C.T. Prewitt, R.M. Hazen, *Am. Mineral*. **1999** ; 84, 245.

[5] M. Tribaudino, M. Prencipe, M. Bruno, D. Levy, *Phys. Chem. Miner.* **2000** ; 27, 656-664

[6] M. Tribaudino, M. Prencipe, F. Nestola, M. Hanfland, *Am. Mineral*. **2001** ; 86, 807.

[7] A. Chopelas, G. Serghiou, *Phys. Chem. Miner*. **2002** ; 29, 403.

[8] F. Nestola, M. Tribaudino, T. Boffa Ballaran, *Am. Mineral*. **2004** ; 89, 189.

[9] F. Nestola, T. Boffa Ballaran, M. Tribaudino, H. Ohashi, *Phys. Chem. Miner*. **2005** ; 32, 222.

[10] F. Nestola, L. Nardini, D. Pasqual, B. Periotto, G. Lucchetti, R. Miletich, D. Belmonte, *Solid State Sci.* **2012** , 14, 1036.

[11] G.D. Gatta, T. Boffa Ballaran, G. Iezzi, *Phys. Chem. Miner*. **2005** ; 32, 132.

[12] R.M. Thompson, R.T. Downs, *Am. Mineral*. **2008** ; 93, 177.

[13] E.S. Posner, P. Dera, R.T. Downs, J.D. Lazarz, P. Irmen, *Phys. Chem. Miner.* **2012** ; 41, 695.

[14] A.B. Woodland, *Geophys. Res. Lett.* **1998** ; 25, 1241.

[15] T. Arlt, R.J. Angel, *Phys. Chem. Miner*. **2000** ; 27, 719.

[16] T. Arlt, R.J. Angel, R. Miletich, T. Armbruster, T. Peters, *Am. Mineral*. **1998** ; 83, 1176.

[17] T. Arlt, M. Kunz, J. Stoltz, T. Armbruster, R.J. Angel, *Contrib. Mineral. Petr*. **2000** ; 138, 35.

[18] A. Ullrich, R. Miletich, T. Balic-Zunic, L. Olsen, F. Nestola, M. Wildner, H. Ohashi, *Phys. Chem. Miner.* **2010** ; 37, 25.

[19] J.S. Zhang, B. Reynard, G. Montagnac, R.C. Wang, J.D. Bass, *Am. Mineral*. **2013** ; 98, 986.

[20] J.S. Zhang, B. Reynard, G. Montagnac, J.D. Bass, *Phys. Earth Planet. In.* **2014** ; 228, 159.

[21] G. Finkelstein, P. Dera, T.S. Duffy, *Phys. Earth Planet. In.* **2015** ; 244, 78.

[22] N.L. Ross, B. Reynard, *Eur. J. Mineral.* **1999** ; 11, 585.

[23] G. Serghiou, *J. Raman Spectrosc*. **2003** ; 34, 587.

[24] C.L.S. Pommier, M.B. Denton, R.T. Downs, *J. Raman Spectrosc*. **2003** ; 34, 769.

[25] E. Huang, C. H. Chen, T. Huang, E. H. Lin, J.A. Xu, *Am. Mineral*. **2000** ; 85, 473.

[26] M. Tribaudino, L. Mantovani, D. Bersani, P.P. Lottici *Am. Mineral*. **2012** ; 97, 1339.

[27] M. Prencipe, L. Mantovani, M. Tribaudino, D. Bersani, P.P. Lottici, *Eur. J. Mineral*. **2012** ; 24, 457.

[28] C. Stangarone, M. Tribaudino, M. Prencipe, P.P. Lottici, *J. Raman Spectros*. **2016** ; 47,1247.

[29] A.M. Plonka, P. Dera, P. Irmen, M.L. Rivers, L. Ehm, J.B. Parise, *Geophys. Res. Lett*. **2012** ; 39.

[30] A.E. Ringwood, M. Seabrook, *J. Geophys. Res*. **1963** ; 68, 4601.

[31] A.E. Ringwood *Phys. Earth Planet. In*. **1970** ; 3, 109.

[32] F. Nestola, G. J. Redhammer, M. G. Pamato, L. Secco, A. Dal Negro, *Am. Mineral*. **2009** ; 94, 616.

[33] G.J. Redhammer, F. Nestola, R. Miletich, *Am. Mineral*. **2012** ; 97, 1213.

[34] G.J. Redhammer, G. Tippelt, *Acta Crystallogr. C*. **2014** ; 70, 852.

[35] G. Hofer, J. Kuzel, K. S. Scheidl, G. Redhammer, R. Miletich, *J. Solid State Chem*. **2015** ; 229, 188.

[36] R. Miletich, D.R. Allan, W.F. Kush, in *High Temperature and High Pressure crystal chemistry* (Eds: R.M. Hazen, R.T. Downs), Reviews in Mineralogy and Geochemistry, Mineralogical Society of America and Geochemical Society, Washington DC, **2000**, pp 445-519.

[37] M. Prencipe, M. Tribaudino, A. Pavese, A. Hoser, M. Reehuis, *Can. Mineral*. **2000** ; 38, 183.

[38] L. Mantovani, M. Tribaudino, F. Mezzadri, G. Calestani, G. Bromiley, *Am. Mineral*. **2013** ; 98, 1241.

[39] L. Mantovani, M. Tribaudino, G. Bertoni, G. Salviati, G. Bromiley, *Am. Mineral*. **2014** ; 99, 704.

[40] E. Lambruschi, I. Aliatis, L. Mantovani, M. Tribaudino, D. Bersani, G. Redhammer, P.P. Lottici, *J. Raman Spectrosc*. **2015** ; 46, 586.

[41] H.K. Mao, J. Xu, P.M. Bell, *J. Geophys. Res*. **1986** ; 91, 4673.

[42] R.J. Angel, M. Bujak, J. Zhao, G.D. Gatta, S.D. Jacobsen, *J. Appl. Cryst.* **2007** ; 40, 26.

[43] J. Etchepare, In *Amorphous materials*, (Eds. R.W. Douglas, B. Ellis), Wiley Interscience, London, **1970**, pp. 337-346.

[44] Y. Hu, P. Dera, K. Zhuravlev, *Phys. Chem. Miner*. **2015** ; 42, 595.

[45] C. Gori, M. Tribaudino, L. Mantovani, F. Mezzadri, D. Delmonte, E. Gilioli, G. Calestani, *Mineral. Mag*. **2016**, accepted.

[46] L. Mantovani, M. Tribaudino, I. Aliatis, E. Lambruschi, D. Bersani, P.P. Lottici, *Phys. Chem. Miner*. **2015** ; 42, 179.

[47] L. Zhang, H. Ahsbahs, S. Hafner, A. Kutoglu, *Am. Mineral*. **1997** ; 82, 245.

[48] J. Glinnemann, H.E. King Jr, H. Schulz, T. Hahn, S.J. La Placa, F. Dacol, *Z. Krist-New Cryst. St.* **1992** ; 198, 177.

[49] A.C. McCarthy, R. T. Downs, R. M. Thompson, G.J. Redhammer, *Am. Mineral*. **2008** ; 93, 1829.

Table 1. Pressure-dependence of the Raman peak positions in silicate pyroxenes. Slope dv_i/dP and intercept from a linear fit are given; strongest peaks in bold. In parentheses: *e.s.d.* of the linear best fit.

$CaMgSi_2O_6$			$CaCoSi_2O_6$			Chopelas and Serghiou [7]	
ν (cm^{-1})	Intercept (cm^{-1})	$\partial\nu/\partial P$ (cm^{-1}/GPa)	ν (cm^{-1})	Intercept (cm^{-1})	$\partial\nu/\partial P$ (cm^{-1}/GPa)	Intercept (cm^{-1})	$\partial\nu/\partial P$ (cm^{-1}/GPa)
323	**324(1)**	**2.8(2)**	**310**	**312(1)**	**2.4(2)**	324.6	3.36
356	**357(1)**	**2.7(2)**	326	328(2)	4.3(5)	356.4	2.98
367	366(1)	3.1(2)	**345**	**346(1)**	**2.8(2)**	365.2	4.01
389	**390(1)**	**3.3(2)**	**375**	**375(1)**	**2.4(2)**	390.2	5.01
667	**665(1)**	**2.9(2)**	**663**	**662(1)**	**2.8(2)**	666.7	3.30
1013	**1012(1)**	**4.4(2)**	**1011**	**1011(1)**	**4.4(2)**	1015.9	4.14

Table 2. Pressure-dependence of the Raman modes in germanate pyroxenes. Slope dv_i/dP and intercept from a linear fit are given; strongest peaks in bold. In parentheses: *e.s.d.* of the linear best fit.

$CaMgGe_2O_6$			$CaCoGe_2O_6$		
ν (cm^{-1})	Intercept (cm^{-1})	$\partial\nu/\partial P$ (cm^{-1}/GPa)	ν (cm^{-1})	Intercept (cm^{-1})	$\partial\nu/\partial P$ (cm^{-1}/GPa)
150	149.0(5)	2.0(1)	155	154.9(5)	0.4(1)
166	168(2)	2.0(6)	165	166.5(7)	1.1(2)
191	191.7(3)	0.8(1)	187		
			262	**263(1)**	**2.6(1)**
275	**275(1)**	**0.9(3)**	285		
297	**294.4(6)**	**3.1(1)**	298		
317	318(1)	2.7(4)	326	324.5(5)	3.4(1)
342	**343(1)**	**2.2(2)**	345		
400	408(2)	4.3(5)	388		
433	431.7(5)	2.9(1)	**423**	**421.2(5)**	**2.5(2)**
553	**551.1(5)**	**3.5(1)**	**547**	**545.7(5)**	**3.4(1)**
726	721(1)	2.9(2)	721		
755			755	754.0(6)	4.7(2)
828	**830(2)**	**3.9(3)**	809	806(2)	5.0(4)
857	**854.7(5)**	**5.3(1)**	**843**	**840.9(5)**	**4.8(1)**

Captions for figures

Fig. 1. Raman spectra of $CaMgSi_2O_6$ (a) and $CaCoSi_2O_6$ (b) at different pressures. The spectra are cut at about 800 cm^{-1}, excluding the region of the ethanol and methanol peaks; (c) example of deconvolution of the highest energy peak of the silicates, shifted from 1010 cm^{-1} at ambient pressure to 1037 cm^{-1} at 5.58 GPa.

Fig. 2. Raman spectra of $CaMgGe_2O_6$ (a) and $CaCoGe_2O_6$ (b) at different pressures.

Fig. 3: Raman peak position changes with pressure increase (cm^{-1}/GPa) of the strong peaks at ~ 660-1010 cm^{-1} ($CaCoSi_2O_6$ and $CaMgSi_2O_6$) and at ~ 550-850 cm^{-1} ($CaCoGe_2O_6$ and $CaMgGe_2O_6$). In silicates the peaks at high wavenumber are superimposed

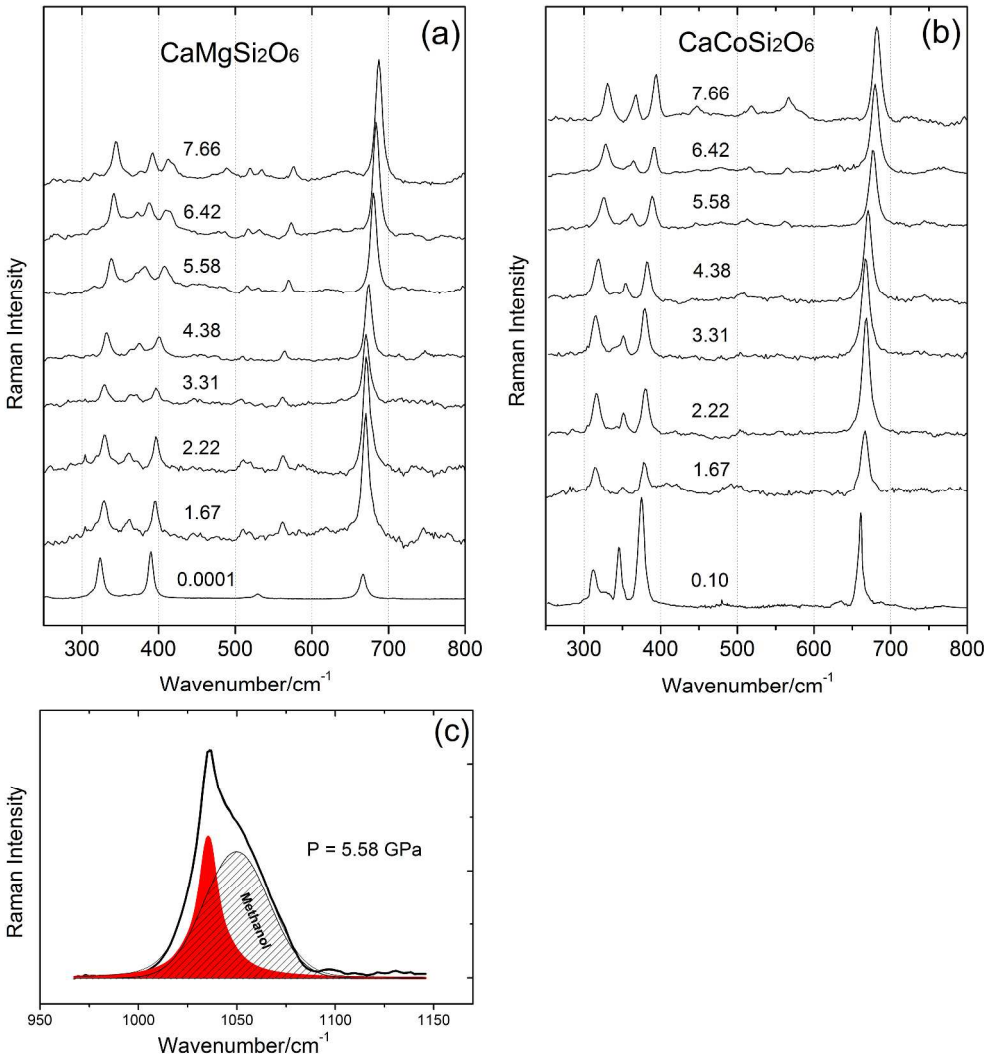

Fig. 1. Raman spectra of $CaMgSi_2O_6$ (a) and $CaCoSi_2O_6$ (b) at different pressures. The spectra are cut at about 800 cm^{-1}, excluding the region of the ethanol and methanol peaks; (c) example of deconvolution of the highest energy peak of the silicates, shifted from 1010 cm^{-1} at ambient pressure to 1037 cm^{-1} at 5.58 GPa.

Fig.1
465x508mm (300 x 300 DPI)

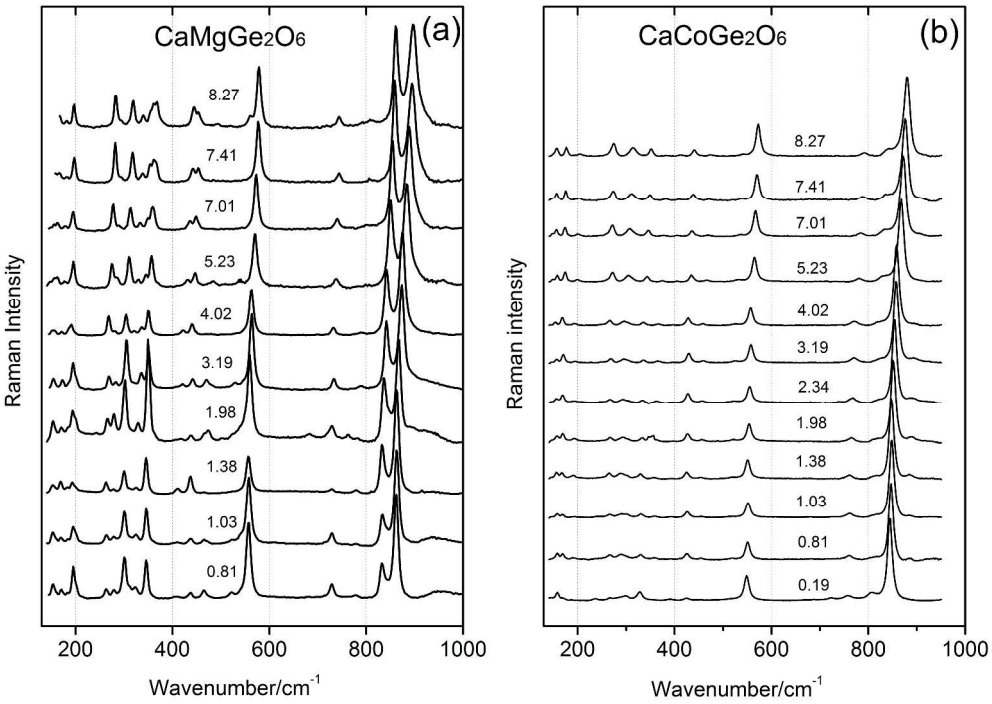

Fig. 2. Raman spectra of $CaMgGe_2O_6$ (a) and $CaCoGe_2O_6$ (b) at different pressures.
Fig.2
578x413mm (300 x 300 DPI)

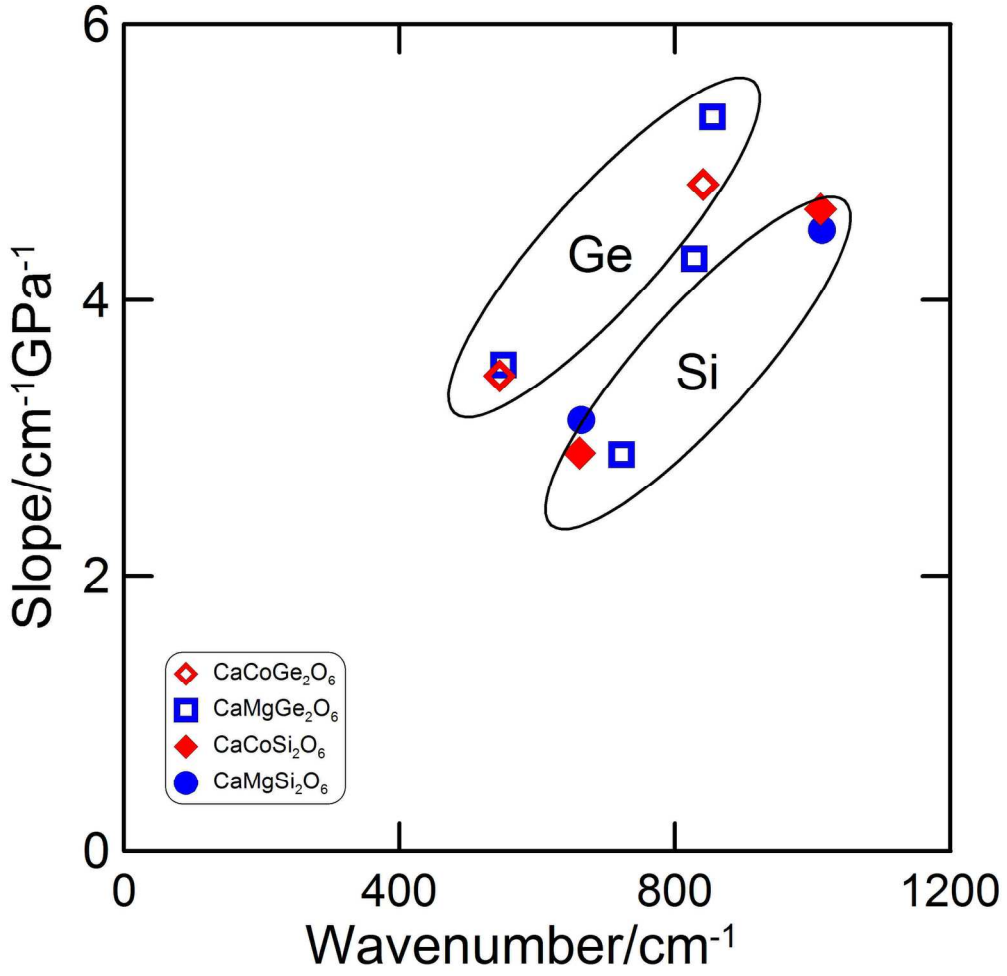

Fig. 3: Raman peak position changes with pressure increase (cm^{-1}/GPa) of the strong peaks at ~ 660-1010 cm^{-1} ($CaCoSi_2O_6$ and $CaMgSi_2O_6$) and at ~ 550-850 cm^{-1} ($CaCoGe_2O_6$ and $CaMgGe_2O_6$). In silicates the peaks at high wavenumber are superimposed.
Fig.3
180x176mm (300 x 300 DPI)